Angular correlation of a pair of Lyman-α photons produced in the photodissociation of H_2

Yuko Nakanishi,[1] Kouichi Hosaka,[1] Ryoko Kougo,[1] Takeshi Odagiri,[2] Motoyoshi Nakano,[1] Yoshiaki Kumagai,[1] Kennichi Shiino,[1] Masashi Kitajima,[1] and Noriyuki Kouchi[1]

[1]*Department of Chemistry, Tokyo Institute of Technology, Meguro-ku, Tokyo 152-8551, Japan*

[2]*Department of Materials and Life Sciences, Sophia University, Chiyoda-ku, Tokyo 102-8554, Japan*

(Received 3 June 2014; revised manuscript received 16 September 2014; published 8 October 2014)

The angular correlation functions (ACFs) of a pair of Lyman-α photons emitted from H fragments in the photodissociation of a hydrogen molecule are measured at a 33.66-eV incident photon energy and at hydrogen gas pressures of approximately 0.1 and 1 Pa. The ACFs are measured for both opposite and nonopposite arrangements of the two photon detectors. It turns out that the experimental ACFs involve neither the contribution of the reactions H($n = 2$) + H_2 nor the contribution of the cascade from H($n \geqslant 3$) to H($2p$) fragments. Thus the experimental ACFs are those for primary H($2p$) pairs following the photodissociation of H_2. The experimental ACFs are compared with (i) the theoretical ACF for entangled pairs of H($2p$) atoms, where the magnetic quantum number of each hydrogen atom is indefinite, and (ii) the theoretical ACF for H($2p$) pairs with definite magnetic quantum number of each hydrogen atom relative to the internuclear axis [the former entangled state of H($2p$) pairs is a sum of the latter pair states with definite magnetic quantum number]. In the theoretical ACF in (ii), the disentanglement in H($2p$) pairs during the dissociation is considered. The experimental ACFs show a similar tendency in angular dependence to the theoretical ACF for entangled H($2p$) pairs. However, there still remains a considerable difference in the variation magnitude between those experimental and theoretical ACFs. The experimental ACFs show the reverse tendency in angular dependence to the theoretical ACF for H($2p$) pairs with definite magnetic quantum number of each hydrogen atom relative to the internuclear axis. We thus conclude that the pair of H($2p$) atoms in the photodissociation of H_2 is unlikely to be in the definite states of magnetic quantum number of each hydrogen atom relative to the internuclear axis, i.e., unlikely to be in the components of the entangled state of H($2p$) pairs.

DOI: 10.1103/PhysRevA.90.043405 PACS number(s): 33.80.Gj

I. INTRODUCTION

Entanglement in massive quantum particles has been intensively studied in atomic ions [1] and neutral atoms [2] to realize quantum information technologies. In most studies, the entangled particles are produced with active control techniques. Odagiri *et al.* [3] found an atom-pair formation process (1) through the coincidence detection of two Lyman-α photons, which are potentially entangled, and measured the cross sections of process (1) against the incident photon energy,

$$\begin{aligned} H_2(X\,^1\Sigma_g{}^+) + \gamma_{ex} &\rightarrow H_2{}^{**}\left[\text{the dissociative } Q_2\,^1\Pi_u(1)\text{state}\right] \\ &\rightarrow H(2p_0) + H(2p_{\pm1}) \\ &\rightarrow H(1s) + H(1s) + \gamma_{Ly-\alpha} + \gamma_{Ly-\alpha}, \quad (1) \end{aligned}$$

where γ_{ex} is the incident photon and $\gamma_{Ly-\alpha}$ the Lyman-α photon. The subscripts of 0 and ±1 attached to $2p$ are the magnetic quantum numbers m with respect to the internuclear axis. Subsequently, Miyagi *et al.* [4] theoretically showed that a pair of H($2p_0$) and H($2p_{\pm1}$) atoms in process (1) is entangled and calculated the angular correlation function (ACF) of the pair of Lyman-α photons emitted by the entangled pair of H($2p$) atoms by means of the two-photon correlation function in quantum optics [5]. Their ACF shows strong contrast, i.e., the visibility amounts to 100% [4]. The molecular photodissociation offers an alternative passive approach to the production of entangled atom pairs. Jänkälä *et al.* [6] calculated the angle-differential cross section for the emission of a pair of fluorescence photons from an entangled atom pair produced in the photodissociation of a diatomic molecule. Their method is based upon the calculation of the transition dipole moments for the absorption of an incident photon and cascading emissions of two photons from a diatomic molecule at an infinite internuclear distance. The angle-differential cross section gives the ACF of a pair of fluorescence photons. As shown later, both ACFs, one by Miyagi *et al.* [4] and the other by Jänkälä *et al.* [6], agree qualitatively. However, the ACF by Jänkälä *et al.* [6] shows weaker contrast than that by Miyagi *et al.* [4]. It follows from the two theories [4,6] that measuring the ACF of the pair of Lyman-α photons results in investigating the state of the H($2p$) pair produced in process (1).

Our group measured the ACFs of the pair of Lyman-α photons in process (1) from the above-mentioned aspect [7,8]. However, previous measurements were limited to the opposite arrangement of two photon detectors [see Fig. 4(a)] since the apparatus was equipped with just one rotation axis. In the present investigation we aim at measuring the ACFs for opposite and nonopposite [see Figs. 4(b) and 4(c)] arrangements with the apparatus where the two photon detectors can independently be rotated around the axis of the incident photon beam and aim at comparing the experimental ACFs with the theoretical predictions [4,6]. It turns out during the present experiment that false coincidence counts probably due to cosmic muons are mixed into the two-photon coincidence counts. In the present experiment the contribution of such false coincidences becomes negligible by using sensitivity-enhanced microchannel plates with CsI coating, while in early experiments [7,8] the contribution was not negligible at the lowest pressure of the hydrogen gas.

II. EXPERIMENT

The experiments were performed at the undulator beamline BL28B [9] and the bending beamline BL20A [10] of the Photon Factory, Institute of Materials Structure Science, KEK. Linearly polarized light was introduced into a gas cell filled with molecular hydrogen. The polarization degree of the incident light from the undulator line BL28B is 0.98 [11] and that from the bending line BL20A is approximately 0.8 [12,13]. The spot size of the incident light beam at the BL28B is much smaller than that at the BL20A, $2 \times 2\,\mathrm{mm}^2$. The incident photon energy was 33.66 eV as in the early experiments [7,8], which gives the maximum value of the cross sections for the emission of the pair of Lyman-α photons [3].

The geometry of the present experiments can be seen in Fig. 1. The space-fixed XYZ frame and body-fixed xyz frame are shown. The Z axis is chosen to lie on the unit polarization vector of the linearly polarized incident light $\hat{\boldsymbol{\varepsilon}}$ and the X axis is chosen to lie along the wave-number vector $\boldsymbol{k}$ of the incident light. The gas cell consists of three coaxial cylinders [14], where the symmetry axis coincides with the $\boldsymbol{k}$ vector of the incident light, i.e., the X axis. The two photon detectors are put on the outermost and innermost cylinders in such a way that the detectors are on the lines perpendicular to the X axis at a distance of 14.5 mm and rotate independently around the X axis. The apparatus is equipped with a double rotation axis. The solid angle subtended by each detector from the origin of the XYZ frame is 0.64 sr, the same as in previous experiments [7,8].

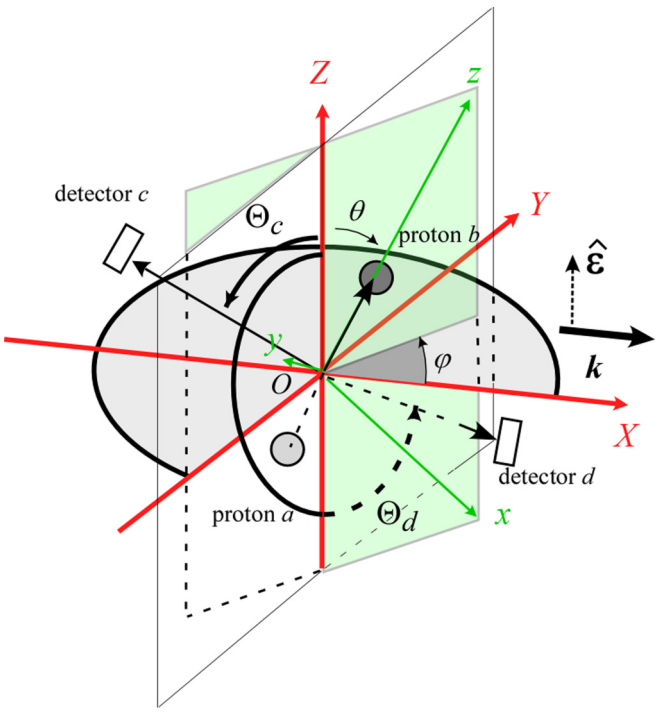

FIG. 1. (Color online) Geometry of the present experiments. The unit polarization vector of the linearly polarized incident light is denoted by $\hat{\boldsymbol{\varepsilon}}$ and the wave number vector of the incident light by $\boldsymbol{k}$. The space-fixed XYZ frame is introduced in such a way that the Z axis is parallel to $\hat{\boldsymbol{\varepsilon}}$ and the X axis is parallel to $\boldsymbol{k}$. The body-fixed xyz frame, where the z axis is the internuclear axis, is introduced against the space-fixed XYZ frame with the Euler angles $(\varphi, \theta, 0)$.

Each photon detector for the vacuum ultraviolet radiation is comprised of an MgF_2 window and microchannel plate (F4655-10, Hamamatsu photonics) coated with CsI, which provides a filter range of approximately 115–200 nm. Only Lyman-α radiation, with a 121.6-nm wavelength, is detected at a 33.66-eV incident photon energy. The microchannel plate without CsI coating used in the early experiments [7,8] was replaced by that with CsI coating to increase the detection efficiency for Lyman-α photons approximately ten times [15], resulting in efficiency two orders of magnitude higher for the coincidence detection of two Lyman-α photons. In fact, the detection efficiency of the microchannel plate with CsI coating was increased three to ten times in the present experiments as compared to that without CsI coating.

The photon detectors are labeled c and d and their directions are expressed by the Euler angles $(\Phi_c, \Theta_c, 0)$ and $(\Phi_d, \Theta_d, 0)$, respectively, provided the detectors are originally on the $+Z$ axis. We note that $\Phi_c = \Phi_d = \frac{3}{2}\pi$ in the present and previous experiments [7,8]. The detectors are hence on the YZ plane, i.e., the plane perpendicular to the incident light beam. The angles Θ_c and Θ_d express the rotation angles around the X axis and their positive direction is the counterclockwise direction when facing into the positive direction of the X axis. The minimum value of $|\Theta_d - \Theta_c|$ is 120°. It was confirmed by ray tracing of the Lyman-α photon that the integral of the product of two solid angles subtended by the detectors c and d over the interaction region, i.e., the geometric factor, is constant irrespective of Θ_c and Θ_d when the alignment of the detectors is good. It was verified experimentally that the geometric factor was kept constant when detectors c and d rotated as mentioned in Sec. III. The alignment of the photon detectors was examined by measuring the angular distribution of photoelectrons from He at an incident photon energy of 33.66 eV since the asymmetry parameter in the angular distribution has been well known to be 2 [16]. The direction of the unit polarization vector of the linearly polarized incident light was experimentally determined by such photoelectron measurements. Two retardation-type electron-energy analyzers are put on the outermost and innermost cylinders for these purposes, which are shifted by 50 mm down the incident light beam from the photon detectors. The ratio of the count rates from detectors c and d was used as a probe of the drift of the alignment.

The detection times of the Lyman-α photon by the detectors c and d, t_c and t_d, respectively, were recorded with a time-to-digital converter (TDC8HP, RoentDek). The width of one channel is 25.1 ps, which was obtained by using two clocks: the time calibrator (Ortec 462) and the timing signal from the storage ring synchronized with the pulsed synchrotron radiation. The number of events that the time difference $t_d - t_c$ is equal to T is counted for a given value of T and plotted against T, which is the two-photon coincidence time spectrum. It is in fact shifted along the T axis because of the instrumental delay time. Figure 2 shows an example measured at a 33.66-eV incident photon energy, 1.4-Pa hydrogen gas pressure, and $(\Theta_c, \Theta_d) = (-90°, 90°)$. In fact, the spectrum in Fig. 2 is on top of the accidental coincidence that reflects the bunch structure in the storage ring, i.e., the bunch-to-bunch interval of

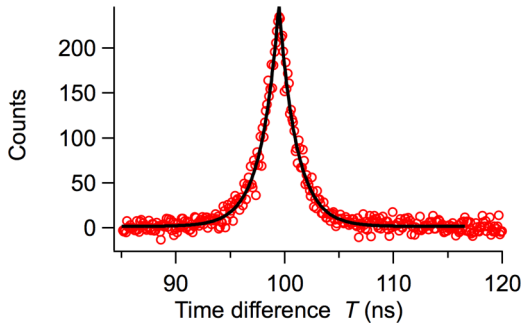

FIG. 2. (Color online) Example of the two-photon coincidence time spectra, which was measured at a 33.66-eV incident photon energy, 1.4-Pa hydrogen gas pressure, and $(\Theta_c,\Theta_d) = (-90^\circ,90^\circ)$. The accidental coincidence has been subtracted. The four channels of the time-to-digital converter are binned to be 0.1004 ns/channel. The solid curve shows the best-fit curve of Eq. (2).

2 ns, the time taken for a bunch to circle the ring, 624 ns, and the fill pattern in the ring. The accidental coincidence including the flat component as well is subtracted by using the fact that it has a period of 624 ns. The peak in Fig. 2 has a decay time constant of 1.6 ns, the lifetime of an H($2p$) atom [17]. There exists a slow component with a time constant of approximately 100 ns underneath the peak. The slow component may be ascribed to the l-changing reaction of H($2s$) fragments produced in the photodissociation [18] and to cascade from H($n \geqslant 3$) to H($2p$) fragments: The lifetime of H($3s$) is 160 ns and that of H($3d$) is 15.6 ns [17,19]. Hence we fitted the function with the fitting parameters of C_1, C_2, T_0, and τ,

$$y(T) = C_1\, e^{-|T-T_0|/\tau} + C_2, \qquad (2)$$

to the experimental two-photon coincidence time spectra in the range of ± 16 ns from T_0 to separate the slow component, which is considered flat in Eq. (2). In fact, the values of C_2 are much smaller than those of C_1. The coincidence rate, which does not include the slow component, is normalized for the incident photon flux and the result is plotted against the hydrogen gas pressure in the gas cell in Fig. 3. The proportional relation is seen in the range up to approximately 1.2 Pa. This is the reason why we normalize the coincidence rate for the hydrogen gas pressure to obtain the ACFs of the pair of the Lyman-α photons, as mentioned later. The proportional relation in Fig. 3 indicates that the coincidence counts obtained with the fitting of Eq. (2) are not affected by the reactions of an H($n = 2$) fragment with an H_2 molecule and the ACFs hardly depend on the hydrogen gas pressure.

The decay time constant τ is in good agreement with the lifetime of an H($2p$) atom, 1.6 ns [17], independent of the hydrogen gas pressures and (Θ_c,Θ_d) in the present range. This result shows that the deexcitation and l-changing reactions of H($2p$) fragments hardly occur within the lifetime of an H($2p$) atom in the present pressure range, which is consistent with the proportional relation in Fig. 3. In conclusion, the two-photon coincidence counts obtained with the fitting of Eq. (2) are free from the reactions H($n = 2$) + H_2 and cascade from H($n \geqslant 3$) to H($2p$) fragments in the present range of hydrogen gas pressure.

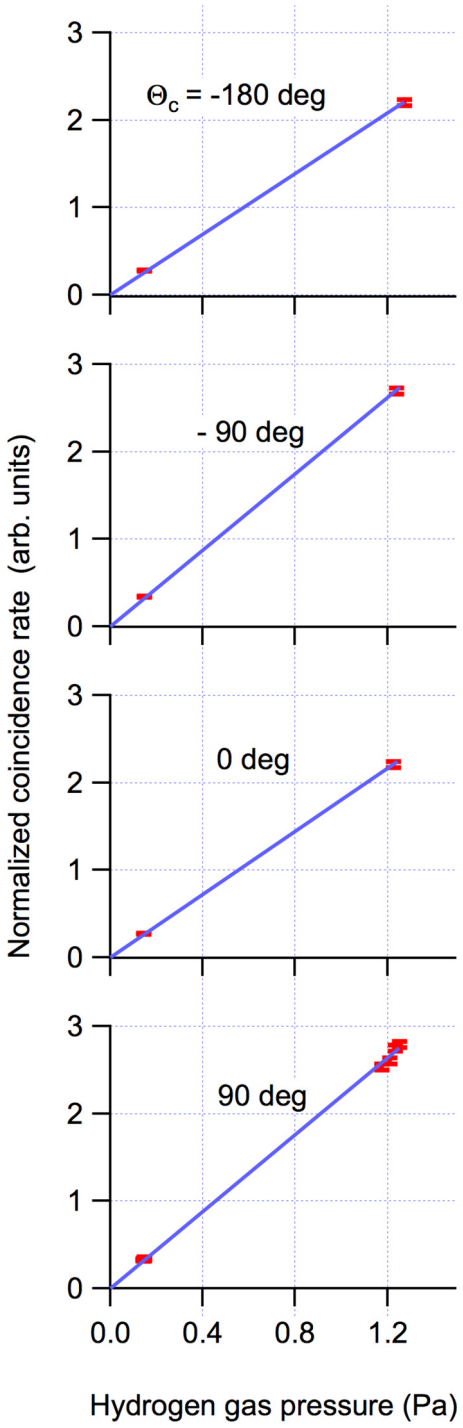

FIG. 3. (Color online) Plot of the coincidence rate normalized for the incident photon flux against the hydrogen gas pressure in the gas cell. Here $\Theta_d = \Theta_c + 180^\circ$, i.e., the opposite arrangement of the two photon detectors [see Fig. 4(a)]. The solid line is the best-fit curve of the proportional relation.

The result of Fig. 3 was obtained with the single-axis apparatus. The hydrogen gas pressure in the cell was almost constant independent of the directions of the photon detectors expressed by (Θ_c,Θ_d). On the other hand, the pressure in the cell depended on (Θ_c,Θ_d) to a much larger extent in the double-axis apparatus than in the single-axis one: The pressure

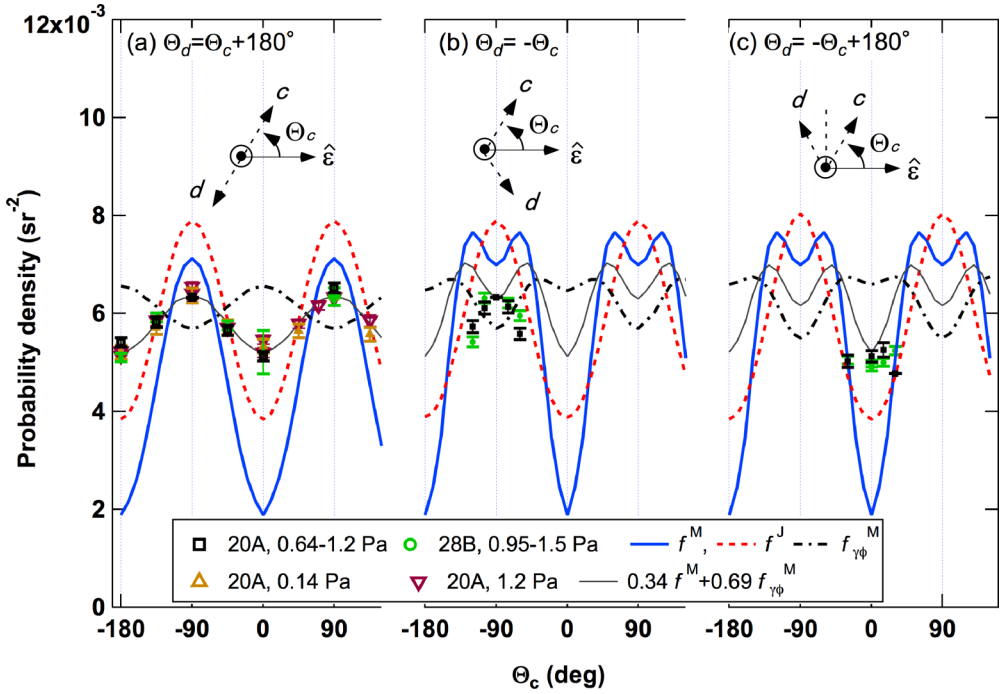

FIG. 4. (Color online) Experimental and theoretical ACFs of a pair of Lyman-α photons following the photodissociation of H_2. The symbols denote the experimental ACFs measured at the incident photon energy of 33.66 eV measured at BL20A (□, △, and ▽) and BL28B (◯). The pressure indicates that of hydrogen gas in the gas cell. Curves show the theoretical ACFs: blue solid curve, f^M [Eq. (11)] [4]; red dashed curve, f^J [Eq. (18)] [6,23]; black dash-dotted curve, $f^M_{\gamma\phi}$ [Eq. (13)] [4]; and thin gray curve, f [Eq. (19)] with $p_1 = 0.34$ and $p_2 = 0.69$.

ranged from 0.64 to 1.2 Pa and 0.95 to 1.5 Pa with changing values of Θ_c and Θ_d in the double-axis apparatus as shown in Fig. 4 (squares and circles), while the pressure was kept constant during the measurement at a given set of Θ_c and Θ_d in the double-axis apparatus. Such a large variation of the pressure from angle to angle in the double-axis apparatus does not matter in the ACF measurement because the coincidence rate is normalized for the hydrogen gas pressure, almost constant at a given angle, based upon the proportional relation in Fig. 3. The large variation of the pressure in the double-axis apparatus is due to the fact that the leak rate of hydrogen gas through the interstices of cylinders in the gas cell is dependent on (Θ_c,Θ_d).

The coincidence rate at a given set of Θ_c and Θ_d, $\dot{N}_{cd}\,(\Theta_c,\Theta_d)$, is normalized for the flux of the incident photons and the hydrogen gas pressure in the gas cell to obtain $\dot{N}_{cd}(\Theta_c,\Theta_d)/(Pi_{\rm Au})$, where P is the hydrogen gas pressure and $i_{\rm Au}$ the photocurrent from the Au plate placed at the back of the gas cell. The reference measurements were carried out at a constant angle of $(\Theta_c,\Theta_d) = (-\frac{\pi}{2},\frac{\pi}{2})$ or $(\frac{\pi}{2},-\frac{\pi}{2})$ to compensate a possible but small and slow change of the geometric factor and the sensitivity of the detectors during the measurement. The reference measurements were carried out before and after the measurement of $\dot{N}_{cd}(\Theta_c,\Theta_d)/(Pi_{\rm Au})$ to obtain $\dot{N}'_{cd}(-\frac{\pi}{2},\frac{\pi}{2})/(P'i'_{\rm Au})$ and $\dot{N}''_{cd}(-\frac{\pi}{2},\frac{\pi}{2})/(P''i''_{\rm Au})$. The value of

$$\frac{\dot{N}_{cd}(\Theta_c,\Theta_d)/(Pi_{\rm Au})}{\frac{1}{2}\left[\left\{\dot{N}'_{cd}\left(-\frac{\pi}{2},\frac{\pi}{2}\right)/(P'i'_{\rm Au})\right\}+\left\{\dot{N}''_{cd}\left(-\frac{\pi}{2},\frac{\pi}{2}\right)/(P''i''_{\rm Au})\right\}\right]} \quad (3)$$

is the relative cross section of process (1) against Θ_c and $\Theta_d(\Phi_c = \Phi_d = \frac{3}{2}\pi)$, differential with respect to each solid angle for the emission of the pair of Lyman-α photons. The plot of the value (3) against Θ_c and Θ_d hence gives the ACF of the pair of Lyman-α photons.

III. RESULTS

The ACFs measured in the present experiment are shown in Fig. 4, where the incident photon energy is 33.66 eV and the hydrogen gas pressures are approximately 0.1 and 1 Pa. The ACFs denoted by up and down triangles have been measured with the single-axis apparatus and those denoted by squares and circles have been measured with the double-axis apparatus. During the present experiment it has turned out that the false coincidence counts coming from outside the vacuum chamber are mixed into the two-photon coincidence counts as mentioned below.

The two-photon coincidence time spectra were measured without introducing the incident light beam and hydrogen gas and some examples of these measurements are shown in Fig. 5. The detectors c and d were opposite to each other on the vertical plane. The angle of c from the vertical line is written as Θ_p (see Fig. 5). When the detector c is at the top and d is at the bottom, Θ_p is 0°. The detectors are on the horizontal line for $\Theta_p = 90°$. The time difference T is equal to $t_d - t_c$, as mentioned in Sec. II. The time spectrum is in fact shifted along the T axis because of the instrumental delay time. The point of $T = 0$ in Fig. 5 is taken at the midpoint of the two peaks for $\Theta_p = 180°$ and 0°. The peak in Fig. 5 is a false coincidence peak and appears to overlap with the real coincidence peak. The decay is much faster than the lifetime of an H($2p$) atom, 1.6 ns [17]. The peak position for $\Theta_p = 180°$, with the detector d

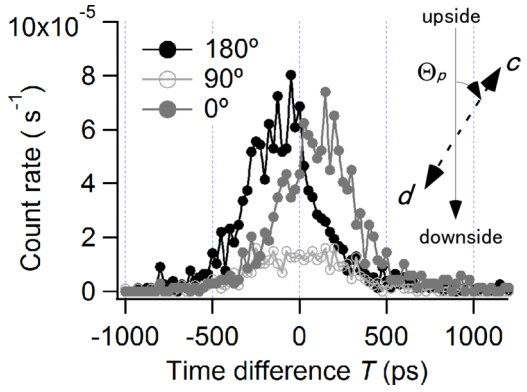

FIG. 5. (Color online) Coincidence time spectra without introducing the incident light and hydrogen gas for $\Theta_p = 0^\circ$ (gray circles), $\Theta_p = 90^\circ$ (white circles), and $\Theta_p = 180^\circ$ (black circles).

is at the top, is earlier than that for $\Theta_p = 0^\circ$, where c is at the top, by approximately 200 ps. This peak shift leads to the conclusion that some particle passes through the top detector first and then the bottom detector with the velocity close to the light velocity, considering the distance between two photon detectors of 14.5 mm × 2.

Figure 6 shows the variation of the count rate of the false coincidence against Θ_p. The sensitivity of the detector for the particle is independent of whether the microchannel plate is coated with CsI or not. The angular distribution in Fig. 6 is consistent with the above-mentioned conclusion that the particle comes from above and is expressed as

$$A\cos^2\Theta_p + B. \tag{4}$$

The solid line in Fig. 6 is the best-fit curve of Eq. (4). It is known as the polar angle distribution of cosmic muons, where the first term $A\cos^2\Theta_p$ is attributed to the primary muons and the second term B to the secondary muons produced through the air shower of the primary cosmic rays [20]. Hence the false coincidences seem to originate from cosmic muons. A $200 \times 200\,\mathrm{mm}^2$ square plastic scintillator

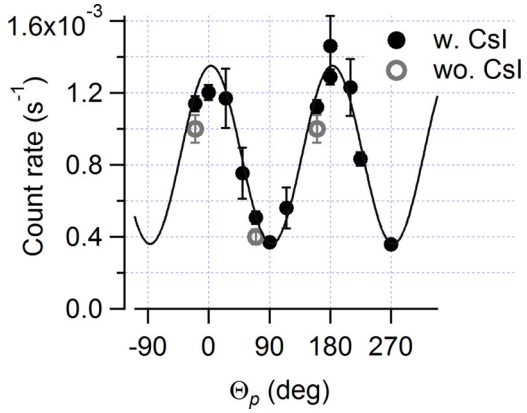

FIG. 6. (Color online) Angular distribution of the false coincidence rate measured through the microchannel plates with (black closed circles) and without (open gray circles) CsI coating. The solid line is the best-fit curve of Eq. (4).

was placed outside the experimental vacuum chamber to verify the origin of the false coincidences. When the plastic scintillator was on top of the chamber and $\Theta_p = 0^\circ$, i.e., the scintillator, detector c, and detector d aligned vertically from the top, triple coincidences among the scintillator signal, detector c signal, and detector d signal were recorded. The ratio of the triple coincidences to the double coincidences between detectors c and d was approximately 40%, which was explained by the straight-line trajectories that simulate the trajectories of muons. In conclusion, the false coincidence counts are probably attributed to cosmic muons. In the present experiments, as the microchannel plates coated with CsI are used, the ratio of the false coincidence counts to the total coincidence counts (false coincidence counts plus real ones) was less than 1% even at the lowest pressure of 0.14 Pa. The ACFs in Fig. 4 are therefore free from false coincidence counts.

The anisotropy of the experimental ACFs is so weak that those ACFs are approximately put on the absolute scale of the vertical axis in Fig. 4 in such a way that the value of the ACF at the angle of reference measurements mentioned in Sec. II is set equal to $\frac{1}{(4\pi)^2}$ in units of sr^{-2}. We note that the integral of the ACF over the entire range of (Φ_c,Θ_c) and (Φ_d,Θ_d) gives unity [see Eq. (12)] and thus the value of the ACF is $\frac{1}{(4\pi)^2}\,\mathrm{sr}^{-2}$ independent of the angles for the isotropic ACF. The arrangements of the two detectors in Fig. 4 are such that (a) $\Theta_d = \Theta_c + 180^\circ$, (b) $\Theta_d = -\Theta_c$, and (c) $\Theta_d = -\Theta_c + 180^\circ$, which are schematically shown in the inset of Fig. 4. The arrangement of detectors in Fig. 4(a) is referred to as the opposite arrangement and those in Figs. 4(b) and 4(c) are nonopposite arrangements. The statistical uncertainty indicated by the error bar is approximately $\frac{1}{3}$ of that in our previous experiments [7,8]. The period of 180° can be clearly seen in Fig. 4(a) as expected, which shows that good alignment was obtained. The ACFs measured at the bending line BL20A are in good agreement with the ACF at the undulator line BL28B. This shows that (i) the anisotropy of the ACF is so weak that the effect of the polarization degree of the incident light, ~0.8 at BL20A and 0.98 at BL28B, as mentioned in Sec. II, is not noticeable and (ii) the geometric factor at BL20A was kept as constant as the geometric factor at BL28B with rotating detectors c and d, although the spot size of the incident light beam at BL20A is much larger than that at BL28B, as mentioned in Sec. II.

In Fig. 4(a) only a small pressure effect can be seen in the range of hydrogen gas pressures of the present experiments (see also Fig. 3). As mentioned in Sec. II, the decay time constant τ in Eq. (2) in the two-photon coincidence time spectrum is in good agreement with the lifetime of an H($2p$) atom, 1.6 ns [17], independent of the hydrogen gas pressures and (Θ_c,Θ_d) in the present range, which is consistent with the prediction by Miyagi *et al.* [4]. On the other hand, Tanabe *et al.* [7,8] reported that with decreasing hydrogen gas pressure from 0.40 to 0.02 Pa, the experimental ACFs for the opposite detector arrangement approached the theoretical ACF by Miyagi *et al.* [4] (blue solid curve in Fig. 4). They also reported that the decay time constant in the two-photon coincidence time spectrum was shortened from the lifetime of an H($2p$) atom, 1.6 ns [17], to half that lifetime with decreasing hydrogen gas pressure from 0.40 to 0.02 Pa. Their ACF and

decay time constant at 0.40 Pa [7,8] are in good agreement with the present results. We measured the ratio of false coincidence counts due to cosmic muons to total coincidence counts (false coincidence counts plus real ones) for the microchannel plates without CsI coating. The ratios were 30%–60% at a 0.02-Pa hydrogen gas pressure and less than 10% at 0.40 Pa. These values would be applicable to the early experiments by Tanabe *et al.* [7,8] since they used the microchannel plate without CsI coating. The pressure effects on the ACF and decay time constant observed in our early experiments [7,8] seem to have been ascribed to the false coincidence counts due to cosmic muons, taking into account (i) the considerable ratio of the false coincidence counts at 0.02 Pa mentioned just above, (ii) the angular distribution of the false coincidence counts (Fig. 6), and (iii) the much faster decay than the lifetime of an H($2p$) atom in the false coincidence time spectra (Fig. 5).

IV. DISCUSSION

As mentioned in Sec. II, the experimental ACFs in Fig. 4 are free from reactions of H($n = 2$) fragments with H_2 molecules and cascade from H($n \geqslant 3$) to H($2p$) fragments because of (i) the fitting of Eq. (2) to eliminate the slow component in the coincidence time spectrum, (ii) the proportional relation in Fig. 3, and (iii) the agreement of the decay time constant τ in Eq. (2) with the lifetime of an H($2p$) atom irrespective of hydrogen gas pressures. Thus the experimental ACFs in Fig. 4 are those of the pair of Lyman-α photons emitted by the primary pair of H($2p$) atoms following the photodissociation of H_2. Before comparing the experimental ACFs with the theoretical ones, let us show that the experimental ACFs in Fig. 4 are free from the reactions of H($n = 2$) fragments also in terms of the cross sections of those reactions since the number of the data points in Fig. 3 is not sufficient. Because the contribution of the l-changing reaction of the H($2s$) fragment is eliminated through the fitting of Eq. (2) and the ACFs are not affected by the deexcitation and l-changing reactions of the H($2p$) fragment, we consider the m-changing reaction

$$\mathrm{H}(2p_m) + \mathrm{H}_2 \rightarrow \mathrm{H}(2p_{m'}) + \mathrm{H}_2. \tag{5}$$

In reaction (5) m is the magnetic quantum number with respect to the internuclear axis [see process (1)] and the partner H($2p$) atom is not shown. Reaction (5) includes all the transformations of states within the $2p$ state.

The mean free time τ_r of the reaction with the cross section of σ_r is given by

$$\tau_r = 1/\sigma_r v n, \tag{6}$$

where v is the relative velocity between a projectile and target and n is the number density of the target. In reaction (5) the H($2p_m$) atom is a projectile and the H_2 molecule is a target. The mean free time of reaction (5) is calculated and compared with the lifetime of H($2p$) atom, 1.6 ns [17], as follows.

The value of v is approximately calculated to be $2.9 \times 10^6\,\mathrm{cm\,s^{-1}}$ from the incident photon energy of 33.66 eV and the dissociation limit of H($2p$) + H($2p$) with respect to the zero-point energy of the H_2 ($X\,^1\Sigma_g{}^+$) molecule, i.e., 24.875 eV [21], since the velocity of an H($2p$) atom against the center of mass of the two protons is much faster than the thermal velocity of an H_2 molecule against the laboratory frame at room temperature. Fleming *et al.* [22] estimated the cross section of reaction (5), σ_{pp}, to be $(1.0 \pm 0.2) \times 10^{-14}\,\mathrm{cm^2}$ from the pressure dependence of the polarization degree of the Lyman-α fluorescence following the photodissociation of H_2 in the range of the incident photon energy from the dissociation limit of H($1s$) + H($2p$) to 0.496 eV above it and found that σ_{pp} is independent of the relative velocity in the range $(2 \times 10^5) - (7 \times 10^5)\,\mathrm{cm\,s^{-1}}$ at 137 K gas temperature. Thus we use their value of σ_{pp} as it is, i.e., $\sigma_{pp} = 1.0 \times 10^{-14}\,\mathrm{cm^2}$ at the relative velocity of $2.9 \times 10^6\,\mathrm{cm\,s^{-1}}$, to calculate the mean free time of reaction (5), τ_{pp}, in the present experiments, which is compared with the lifetime of H($2p$) atom, 1.6 ns [17]. We obtain

$$\tau_{pp} = 93\,\mathrm{ns} \tag{7}$$

at a 1.5-Pa hydrogen gas pressure, the highest pressure in the present experiment. The mean free time of reaction (5) is approximately 58 times the lifetime of H($2p$) atom even at the highest pressure in the present experiments. The experimental ACFs in Fig. 4 are not influenced by the m-changing reaction (5).

It is worth considering the elastic collision of an H($2p$) atom with an H_2 molecule since the elastic collision changes the direction of motion of H($2p$) atoms [23]. Krstić and Schultz [24] reported the cross section of the elastic collision between an H($1s$) atom and H_2 molecule in the range of relative velocity from 5.4×10^5 to $1.7 \times 10^7\,\mathrm{cm\,s^{-1}}$. Hishinuma [25] also reported the cross section of the elastic collision of an H($1s$) atom in the range of relative velocity $(1 \times 10^5) - (1 \times 10^6)\,\mathrm{cm\,s^{-1}}$. The former cross section is approximately four times the latter cross section at $5.4 \times 10^5\,\mathrm{cm\,s^{-1}}$. We use the cross section of $1 \times 10^{-13}\,\mathrm{cm^2}$ for the elastic collision between an H($2p$) atom and H_2 molecule at the relative velocity of $2.9 \times 10^6\,\mathrm{cm\,s^{-1}}$, which is obtained from the elastic collision cross section of H($1s$) atom at $2.9 \times 10^6\,\mathrm{cm\,s^{-1}}$ [24] multiplied by 11, i.e., the squared ratio of the radius of the H($2p$) atom to that of the H($1s$) atom. The mean free time at 1.5 Pa is 9 ns, approximately 6 times the lifetime of the H($2p$) atom. The experimental ACFs in Fig. 4 seem not to be influenced by the elastic collision of an H($2p$) atom with an H_2 molecule quite so much. In fact, the ACF at 0.14 Pa is in good agreement with that at 1.2 Pa, as can be seen in Fig. 4(a). The above-mentioned discussion supports the conclusion that the experimental ACFs in Fig. 4 are those of the pair of Lyman–α photons emitted by the primary pair of H($2p$) atoms following the photodissociation of H_2.

A. Comparison with the theoretical angular correlation functions of a pair of Lyman-α photons

We compare the experimental ACFs with the theoretical ACFs for primary H($2p$) pairs in Fig. 4 and thus the latter are summarized here. According to Miyagi *et al.* [4], the precursor doubly excited state in process (1), where the incident light is linearly polarized, has $^1\Pi_u^+$ symmetry. The plus superscript means that

$$\sigma_{xz} \left|{}^1\Pi_u{}^+\right\rangle = \left|{}^1\Pi_u{}^+\right\rangle, \tag{8}$$

where the operator σ_{xz} is a reflection operator at the xz plane. As shown in Fig. 1, the xz plane is determined by the internuclear axis (the z axis) and the unit polarization vector of the linearly polarized incident light (the Z axis). The $|^1\Pi_u{}^+\rangle$ state is expressed as

$$\begin{aligned}&\left|^1\Pi_u{}^+; r\to+\infty\right\rangle\\&=\frac{1}{2\sqrt{2}}\left[\left|2p_1^a(1)\right\rangle\otimes\left|2p_0^b(2)\right\rangle+\left|2p_1^a(2)\right\rangle\otimes\left|2p_0^b(1)\right\rangle\right.\\&\quad-\left|2p_0^a(1)\right\rangle\otimes\left|2p_1^b(2)\right\rangle-\left|2p_0^a(2)\right\rangle\otimes\left|2p_1^b(1)\right\rangle\\&\quad-\left|2p_{-1}^a(1)\right\rangle\otimes\left|2p_0^b(2)\right\rangle-\left|2p_{-1}^a(2)\right\rangle\otimes\left|2p_0^b(1)\right\rangle\\&\quad\left.+\left|2p_0^a(1)\right\rangle\otimes\left|2p_{-1}^b(2)\right\rangle+\left|2p_0^a(2)\right\rangle\otimes\left|2p_{-1}^b(1)\right\rangle\right]\end{aligned}\tag{9}$$

at infinite internuclear distance, i.e., $r\to+\infty$, where two protons are labeled a and b and two electrons are labeled 1 and 2. The subscripts 0 and ±1 attached to $2p$ are the magnetic quantum numbers m with respect to the internuclear axis. The pair of hydrogen atoms in Eq. (9) is entangled since the magnetic quantum number of each hydrogen atom is indefinite. The entangled H($2p$) pair in Eq. (9) emits an entangled pair of Lyman-α photons expressed as

$$|\Psi\rangle=\tfrac{1}{2}\{(|\gamma_a\phi_b\rangle-|\phi_a\gamma_b\rangle)-(|\rho_a\phi_b\rangle-|\phi_a\rho_b\rangle)\},\tag{10}$$

where the ket vectors $|\gamma\rangle$, $|\phi\rangle$, and $|\rho\rangle$ are single-photon states of the Lyman-α fluorescence generated through the $2p\to1s$ transition in an H atom with $\Delta m=-1$, 0, and 1, respectively. Equation (10) is the photon-pair state emitted by the entangled H($2p$) pair in Eq. (9) with its internuclear axis facing in the direction specified by θ and φ (see Fig. 1). The two-photon correlation function in quantum optics [5] was calculated for the photon-pair state $|\Psi\rangle$ in Eq. (10) against (φ,θ), and then the result was averaged with the weight of the $\Sigma\to\Pi$ excitation probability density of the fixed-in-space molecule, i.e., the weight of $\frac{3}{8\pi}\sin^2\theta$. This means that Miyagi *et al.* [4] calculated the ACF of the pair of Lyman-α photons for randomly oriented H_2 molecules under the axial recoil approximation. The obtained ACF for $\Phi_c=\Phi_d=\frac{3}{2}\pi$ is expressed as [4]

$$\begin{aligned}&f^M\left(\Theta_c,\ \Phi_c=\frac{3}{2}\pi,\ \Theta_d,\ \Phi_d=\frac{3}{2}\pi\right)\\&=\frac{9}{512\pi^2}\{3-\cos2\Theta_c-\cos2\Theta_d\\&\quad-\cos2(\Theta_c-\Theta_d)\}.\end{aligned}\tag{11}$$

The detectors c and d are on the plane perpendicular to the incident light beam for $\Phi_c=\Phi_d=\frac{3}{2}\pi$, as mentioned in Sec. II. Such a plane is referred to as the dipole plane [6]. In the present experiments we measure the ACFs at the dipole plane, as mentioned in Sec. II. The ACF $f^M(\Theta_c,\Phi_c,\Theta_d,\Phi_d)$ is normalized to unity such that

$$\int f^M(\Theta_c,\Phi_c,\Theta_d,\Phi_d)d\Omega_c d\Omega_d=1.\tag{12}$$

Equation (11) is the result of the normalization. The entangled H($2p$) pairs in Eq. (9) give the normalized ACF (11).

Miyagi *et al.* [4] also calculated the ACFs for each term in Eq. (10), i.e., the $|\gamma_a\phi_b\rangle$, $|\phi_a\gamma_b\rangle$, $|\rho_a\phi_b\rangle$, and $|\phi_a\rho_b\rangle$ photon-pair states. Those nonentangled states of the photon pair give the same ACF expressed as [4]

$$\begin{aligned}&f^M_{\gamma\phi}\left(\Theta_c,\Phi_c=\frac{3}{2}\pi,\Theta_d,\Phi_d=\frac{3}{2}\pi\right)\\&=\frac{9}{8960\pi^2}\{62+3\cos2\Theta_c+3\cos2\Theta_d\\&\quad-4\cos2(\Theta_c-\Theta_d)\}.\end{aligned}\tag{13}$$

Equation (13) is the result of averaging with the weight of $\frac{3}{8\pi}\sin^2\theta$ and normalization according to Eq. (12). The photon pairs in the $|\gamma_a\phi_b\rangle$, $|\phi_a\gamma_b\rangle$, $|\rho_a\phi_b\rangle$, and $|\phi_a\rho_b\rangle$ states, the origin of Eq. (13), are emitted by H($2p$) pairs in the first two terms, the third and fourth terms, the fifth and sixth terms, and the seventh and eighth terms in the entangled H($2p$) pair state of Eq. (9), respectively:

$$\left|2p_1^a(1)\right\rangle\otimes\left|2p_0^b(2)\right\rangle+\left|2p_1^a(2)\right\rangle\otimes\left|2p_0^b(1)\right\rangle,\tag{14}$$

$$-\left[\left|2p_0^a(1)\right\rangle\otimes\left|2p_1^b(2)\right\rangle+\left|2p_0^a(2)\right\rangle\otimes\left|2p_1^b(1)\right\rangle\right],\tag{15}$$

$$-\left[\left|2p_{-1}^a(1)\right\rangle\otimes\left|2p_0^b(2)\right\rangle+\left|2p_{-1}^a(2)\right\rangle\otimes\left|2p_0^b(1)\right\rangle\right],\tag{16}$$

$$\left|2p_0^a(1)\right\rangle\otimes\left|2p_{-1}^b(2)\right\rangle+\left|2p_0^a(2)\right\rangle\otimes\left|2p_{-1}^b(1)\right\rangle.\tag{17}$$

Those four states of H($2p$) pairs [Eqs. (14)–(17)] are states with definite magnetic quantum number of each hydrogen atom relative to the internuclear axis in contrast to the entangled state of H($2p$) pairs in Eq. (9). The magnetic quantum number of each hydrogen atom is indefinite in Eq. (9). The H($2p$) pairs in Eqs. (14)–(17) give the same normalized ACF (13).

Jänkälä *et al.* [6,23] calculated the angle-differential cross section for the emission of a pair of fluorescence photons from an entangled atom pair produced in the photodissociation of a diatomic molecule, which gives the ACF of a pair of fluorescence photons. They calculated the three transition dipole moments for the absorption of a linearly polarized incident photon, the emission of the first fluorescence photon by a pair of fragment atoms, and the emission of the second fluorescence photon. The products of the three dipole moments were summed over the possible excitation and emission pathways. The absolute square of the summation gives the angle-differential cross section. The coherent summation comes from the entangled atom pair. The wave function of the pair of H($2p$) atoms in process (1) is not explicitly shown in Ref. [6]. The ACF at the dipole plane calculated for randomly oriented H_2 molecules is expressed as [6,23]

$$\begin{aligned}&f^J\left(\Theta_c,\Phi_c=\frac{3}{2}\pi,\Theta_d,\Phi_d=\frac{3}{2}\pi\right)\\&=\frac{9}{17\,920\pi^2}\{111-25\cos2\Theta_c-25\cos2\Theta_d\\&\quad+3\cos2(\Theta_c-\Theta_d)\},\end{aligned}\tag{18}$$

which was normalized to unity according to Eq. (12). In what follows $\Phi_c=\Phi_d=\frac{3}{2}\pi$ is omitted in the expression of ACFs in such a way that we have $f^M(\Theta_c,\Theta_d)$, $f^M_{\gamma\phi}(\Theta_c,\Theta_d)$, and $f^J(\Theta_c,\Theta_d)$ for simplicity.

The theoretical ACF for the entangled H($2p$) pairs in Eq. (9) by Miyagi *et al.* [4] [Eq. (11)] was convoluted with the angular resolution in the present experiments and the result is shown

by the blue solid curve in Fig. 4. The theoretical ACF for entangled H(2p) pairs by Jänkälä *et al.* [6,23] [Eq. (18)] was also convoluted with the present angular resolution and the result is shown by the red dashed curve in Fig. 4. Both ACFs agree qualitatively, while the ACF by Jänkälä *et al.* [6,23] (red dashed curve) shows weaker contrast than that by Miyagi *et al.* [4] (blue solid curve). Miyagi *et al.* [4] treated the detection of a photon pair in a quantal manner, while Jänkälä *et al.* [6] treated it in a classical manner. There is a possibility that the entanglement in the pair of H(2p) atoms in Eq. (9) is broken during the dissociation and the nonentangled photon pair, i.e., each term in Eq. (10), is emitted. As mentioned previously, the $|\gamma_a\phi_b\rangle$, $|\phi_a\gamma_b\rangle$, $|\rho_a\phi_b\rangle$, and $|\phi_a\rho_b\rangle$ photon pairs, i.e., each term in Eq. (10), are emitted by the H(2p) pairs in the first two terms [Eq. (14)], the third and fourth terms [Eq. (15)], the fifth and sixth terms [Eq. (16)], and the seventh and eighth terms [Eq. (17)] in the entangled H(2p) pair state of Eq. (9), respectively. Those four states of H(2p) pairs, Eqs. (14)–(17), are states with definite magnetic quantum number of each hydrogen atom relative to the internuclear axis in contrast to the entangled state of the H(2p) pairs in Eq. (9). The magnetic quantum number of each hydrogen atom is indefinite in Eq. (9). All such H(2p) pairs of definite magnetic quantum number for each hydrogen atom, i.e., all H(2p) pairs in the first two terms, the third and fourth terms, the fifth and sixth terms, and the seventh and eighth terms in the entangled H(2p) pair state of Eq. (9), give the same ACF (13). Equation (13) was convoluted with the present angular resolution and the result is shown by the black dash-dotted curve in Fig. 4.

The experimental ACFs show a shift of 90° as compared to the theoretical ACF for H(2p) pairs with the definite magnetic quantum number of each hydrogen atom relative to the internuclear axis (the black dash-dotted curve in Fig. 4). We thus conclude that the pair of H(2p) atoms in process (1) is unlikely to be in the definite states of magnetic quantum number of each hydrogen atom relative to the internuclear axis, i.e., unlikely to be in the first two terms, the third and fourth terms, the fifth and sixth terms, and the seventh and eighth terms in the entangled H(2p) pair state of Eq. (9). The experimental ACFs do not show this 90° shift as compared to the theoretical ACFs for entangled H(2p) pairs [the blue solid and red dashed curves; the blue solid curve originates from the entangled H(2p) pairs in Eq. (9)]. However, there still remains a considerable difference in the variation magnitude between those experimental and theoretical ACFs.

The smaller variation of the experimental ACFs with angles as compared to the theoretical ACFs for entangled H(2p) pairs [the blue solid curve for the entangled H(2p) pairs in Eq. (9) and red dashed curve] shown in Fig. 4(a) may be explained by a mixture of the entangled H(2p) pairs [Eq. (9)] and the H(2p) pairs in the first two terms, the third and fourth terms, the fifth and sixth terms, and the seventh and eighth terms in the entangled H(2p) pair state of Eq. (9). We consider the partial disentanglement in H(2p) pairs in Eq. (9) during the dissociation. Thus we first tried to fit

$$f(\Theta_c,\Theta_d;p_1,p_2)=p_1 f^M(\Theta_c,\Theta_d)+p_2 f^M_{\gamma\phi}(\Theta_c,\Theta_d) \quad (19)$$

to the experimental ACFs in Fig. 4(a). The entangled H(2p) pairs [Eq. (9)] give the ACF of $f^M(\Theta_c,\Theta_d)$ in Eq. (11) and all H(2p) pairs in the first two terms, the third and fourth terms, the fifth and sixth terms, and the seventh and eighth terms in Eq. (9) give the same ACF $f^M_{\gamma\phi}(\Theta_c,\Theta_d)$ in Eq. (13), as mentioned before. A good fit was obtained with $p_1 = 0.34$ and $p_2 = 0.69$, as shown by the thin gray curve in Fig. 4(a), where $p_1 + p_2$ is almost unity, as expected. However, this set of p_1 and p_2 did not give a good fit in Figs. 4(b) and 4(c) in terms of the shape and magnitude as shown by the thin gray curve. The ACF in an extensive angular range gives a strict examination for theories. We then tried to fit Eq. (19) to all the experimental ACFs in Figs. 4(a)–4(c) to find that there are no sets of p_1 and p_2 reproducing the experimental ACFs simultaneously. The idea mentioned above is not the case.

V. CONCLUSION

We have measured the angular correlation functions of a pair of Lyman-α photons following the photodissociation of H_2 with linearly polarized incident light at a photon energy of 33.66 eV and at hydrogen gas pressures of approximately 0.1 and 1 Pa. The ACFs have been measured not only for the opposite arrangement of the two photon detectors, but also for the nonopposite arrangements.

The present ACFs are free from the false coincidence counts probably due to cosmic muons, which were found in the present experiments. The present ACFs involve neither the contribution of the reactions of H(2p) and H(2s) fragments with H_2 molecules nor the contribution of the cascade from H($n \geqslant 3$) to H(2p) fragments and hence the present ACFs originate from primary H(2p) pairs following the photodissociation of H_2. The pressure effects on the ACF and decay time constant in the coincidence time spectrum are not seen. The pressure effects on the ACF and decay time constant observed in the early experiments [7,8] in the range of a hydrogen gas pressure 0.02–0.40 Pa seem to have been ascribed to the false coincidences due to cosmic muons.

The experimental ACFs have been compared with (i) the theoretical ACF [4] for the entangled pairs of H(2p) atoms in Eq. (9), where the magnetic quantum number of each hydrogen atom is indefinite, and (ii) the theoretical ACF [4] for the H(2p) pairs with the definite magnetic quantum number of each hydrogen atom relative to the internuclear axis, i.e., the theoretical ACF for the H(2p) pairs in the first two terms, the third and fourth terms, the fifth and sixth terms, and the seventh and eighth terms in the entangled H(2p) pair state of Eq. (9). In the theoretical ACF in (ii), we considered the disentanglement in H(2p) pairs in Eq. (9) during the dissociation. The experimental ACFs have also been compared with the theoretical ACF for entangled H(2p) pairs [6,23], which was calculated with a different method from Ref. [4]. The experimental ACFs show a similar tendency in angular dependence to the theoretical ACFs for entangled H(2p) pairs [4,6,23], one of which is the ACF for the entangled H(2p) pairs in Eq. (9). However, there still remains a considerable difference in the variation magnitude between those experimental and theoretical ACFs. The experimental ACFs show the reverse tendency in angular dependence to the theoretical ACF for the H(2p) pairs with the definite magnetic quantum number of each hydrogen atom relative to the internuclear axis [4]. In conclusion, the pair of H(2p)

atoms in process (1) is unlikely to be in the definite states of magnetic quantum number of each hydrogen atom relative to the internuclear axis, i.e., unlikely to be in the components in the entangled H($2p$) pair state of Eq. (9).

ACKNOWLEDGMENTS

The experiment was carried out under the approval of the Photon Factory Program Advisory Committee for Proposal No. 2012G045. This work was supported by Grants-in-Aid for Scientific Research (B) (No. 23350003) and (C) (No. 24550013) from the Japan Society for the Promotion of Science. The authors are grateful to Dr. Arno Ehresmann and Dr. Kari Jänkälä for helpful discussion and providing us with the explicit form of their ACF as a function of four angles. The authors are also indebted to Dr. Isao H. Suzuki for his contribution to the present experiments.

[1] R. Blatt and D. Wineland, Nature (London) **453**, 1008 (2008).
[2] I. Bloch, Nature (London) **453**, 1016 (2008).
[3] T. Odagiri, M. Murata, M. Kato, and N. Kouchi, J. Phys. B **37**, 3909 (2004).
[4] H. Miyagi, A. Ichimura, and N. Kouchi, J. Phys. B **40**, 617 (2007).
[5] M. O. Scully and M. S. Zubairy, *Quantum Optics* (Cambridge University Press, Cambridge, 1997), p. 33.
[6] K. Jänkälä, P. V. Demekhin, S. Heinäsmäki, I. Haar, R. Hentges, and A. Ehresmann, J. Phys. B **43**, 065104 (2010).
[7] T. Tanabe, T. Odagiri, M. Nakano, I. H. Suzuki, and N. Kouchi, Phys. Rev. Lett. **103**, 173002 (2009).
[8] T. Tanabe, T. Odagiri, M. Nakano, Y. Kumagai, I. H. Suzuki, M. Kitajima, and N. Kouchi, Phys. Rev. A **82**, 040101(R) (2010).
[9] K. Amemiya and T. Ohta, J. Synchrotron Radiat. **11**, 171 (2004).
[10] K. Ito, Y. Morioka, M. Ukai, N. Kouchi, Y. Hatano, and T. Hayaishi, Rev. Sci. Instrum. **66**, 2119 (1995).
[11] H. Kimura, T. Kinoshita, S. Suzuki, T. Miyahara, and M. Yamamoto, Proc. SPIE **2010**, 37 (1994).
[12] Y. Hikosaka, T. Aoto, R. I. Hall, and K. Ito, J. Phys. B **36**, 1423 (2003).
[13] T. Aoto, Y. Hikosaka, R. I. Hall, K. Ito, J. Fernández, and F. Martín, Chem. Phys. Lett. **389**, 145 (2004).
[14] D. C. Lorents and W. Aberth, Phys. Rev. **139**, A1017 (1965).
[15] C. Martin and S. Bowyer, Appl. Opt. **21**, 4206 (1982).
[16] V. Schmidt, *Electron Spectrometry of Atoms Using Synchrotron Radiation* (Cambridge University Press, Cambridge, 1997), pp. 43–45, 273–277.
[17] H. A. Bethe and E. E. Salpeter, *Quantum Mechanics of One- and Two-Electron Atoms* (Plenum, New York, 1977), p. 266.
[18] N. Terazawa, M. Ukai, N. Kouchi, K. Kameta, Y. Hatano, and K. Tanaka, J. Chem. Phys. **99**, 1637 (1993).
[19] S. Lauer, H. Liebel, F. Vollweiler, O. Wilhelmi, R. Kneip, E. Flemming, H. Schmoranzer, and M. Glass-Maujean, J. Phys. B **31**, 3049 (1998).
[20] Particle data group, http://pdg.lbl.gov/2013/reviews/rpp2012-rev-cosmic-rays.pdf.
[21] T. E. Sharp, Atomic Data and Nuclear Data Tables **2**, 119 (1970).
[22] E. Flemming, O. Wilhelmi, H. Schmoranzer, and M. Glass-Maujean, J. Chem. Phys. **103**, 4090 (1995).
[23] K. Jänkälä and A. Ehresmann (private communication).
[24] P. S. Krstić and D. R. Schultz, Phys. Rev. A **60**, 2118 (1999).
[25] N. Hishinuma, J. Phys. Soc. Jpn. **41**, 1733 (1976).